16

Mechanical Testing

CHAPTER PREVIEW

The concepts of stress and strain and the elastic moduli should already be familiar. Where ceramics differ from most metals and polymers is that at room temperature most of them are brittle. Flaws play a major, often dominating, role in the mechanical behavior of ceramics. As a result, obtaining properties such as elastic moduli is often more difficult than it would be for metals: preparing the sample can lead to the introduction of flaws. Stress–strain curves for ceramics are usually obtained using a bending test rather than a tensile test. We need only to make our ceramic into a rectangular block. The brittle behavior of ceramics gives them low fracture toughness, a property that can most conveniently be obtained from indentation testing. A key point from this chapter is that when we use ceramics in load-bearing applications we need to understand the importance of flaws and how to incorporate them into our design approach.

16.1 PHILOSOPHY

The classical view of ceramic materials includes the following:

1. They are brittle.
2. Dislocations are not important because they do not move.
3. They are polycrystalline and fracture along grain boundaries.

Once again the classical view of ceramics and many of our preconceived ideas of how they behave are not always correct.

- We can bend a sheet of silicon into a tube.
- We can bend an alumina fiber into a circle.
- Dislocations move ahead of crack tips, are present at heterojunctions, and can be produced in large numbers during single-crystal growth.
- Single-crystal ceramics also fracture (Figure 16.1 shows an Nd-doped YAG single-crystal boule that fractured during growth).

The modern view of ceramics is therefore very different:

1. We may be using the ceramic as a thin film where stresses may be very high.
2. Deformation at high temperatures may be important.
3. In some special "new" ceramics, displacive transformations become important.

It will be important to keep these ideas in mind when you read older texts. We are not going to provide a treatise on mechanical properties of ceramics. There are many existing books that do and some of these are listed at the end of the chapter. What we will do is look at what is special for ceramics.

The general need is to understand the response of a material to an applied stress. The stress may be applied externally or induced by altering other parameters such as temperature (which can cause a phase transformation). The fundamental idea is the link to bonding. In Chapter 4 we described how the Young's modulus is related directly to the bond-energy curve. In Chapter 12 we described the nature of dislocations in ceramics.

So the following three chapters have three special themes

- Mechanical testing—how to do it plus the fundamentals of elastic constants, etc.
- Plastic deformation and how it is accommodated
- Fracture and how to control it

The starting point for most discussions of mechanical properties of materials is a stress–strain (σ–ε) curve for a material in tension. Figure 16.2 shows σ–ε curves for three different materials at room temperature.

Material I: This has a high Young's modulus, high failure stress, low ductility, low toughness, and fractures without significant plastic deformation. **This behavior is characteristic of many ceramics.**

FIGURE 16.1 Cracking in an Nd-doped YAG boule.

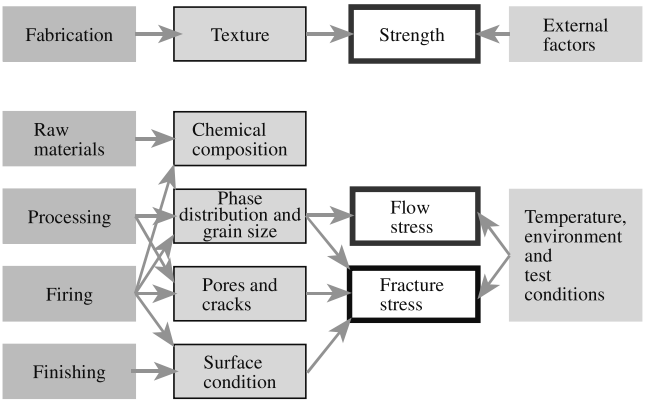

FIGURE 16.3 Factors affecting the mechanical properties of ceramics.

limited toughness. **This behavior is characteristic of many elastomers**.

The strength of ceramics is affected by many factors, and this complexity is illustrated in Figure 16.3. The composition and microstructure are particularly significant and mechanical properties depend strongly on these characteristics. Figure 16.4 shows two specific examples that

Material II: This has moderate strength, moderate ductility, deforms plastically prior to failure, and is the toughest of the three. **This behavior is characteristic of many metals**.

Material III: This has a low Young's modulus, is very ductile, and has low ultimate tensile strength and

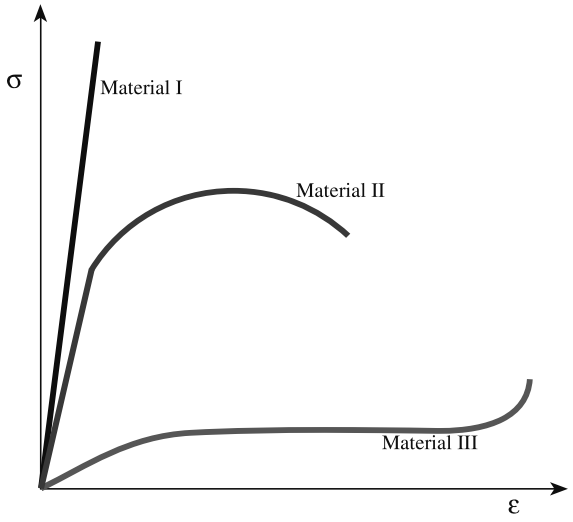

FIGURE 16.2 Idealized stress–strain curves for different materials classes.

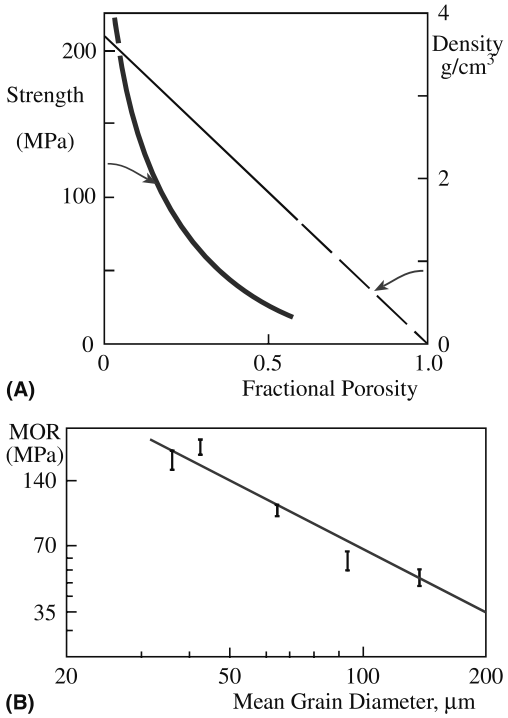

FIGURE 16.4 (a) Effect of porosity on the strength of polycrystalline Al_2O_3. (b) Effect of grain size on the strength of BeO.

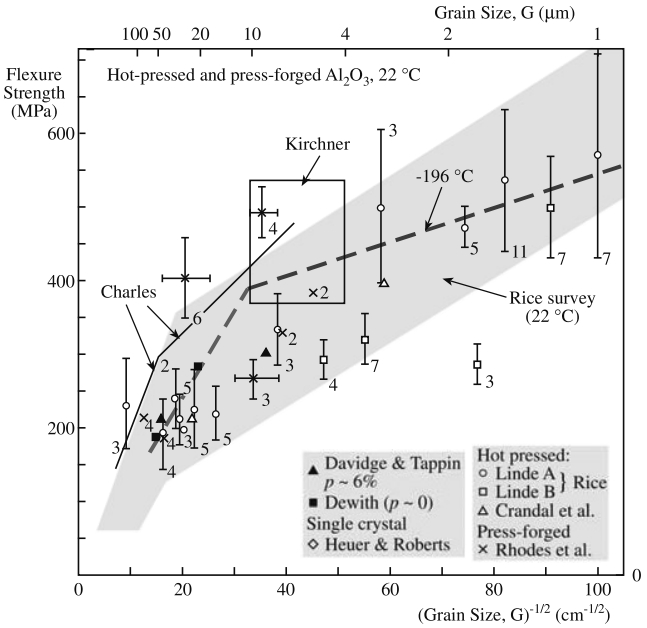

FIGURE 16.5 Compilation of strength data as a function of grain size for polycrystalline Al_2O_3.

illustrate the role of microstructure on the strength of ceramics. In Figure 16.4a the strength of a porous polycrystalline alumina is shown to decrease much more rapidly than its density. The reason is that pores act to concentrate stress, which will not be uniform throughout the ceramic. The strength of nonporous ceramics decreases with increasing grain size as illustrated for the case of BeO in Figure 16.4b. Again, the observed behavior is due to flaws in the material that act as stress concentrators. In large grains there can be larger flaws. The effect of grain size is often more complicated than that shown in Figure 16.4b when we consider ceramics in which the grain size is just a few micrometers. Figure 16.5 is a compilation of flexural strength results for polycrystalline alumina at room temperature as a function of grain size. Despite the considerable scatter in the data, there are clearly two distinct regions. In both cases strength is proportional to the reciprocal square root of the grain size ($d^{-1/2}$) with different constants of proportionality. The reason for this behavior is that in addition to the preexisting flaws causing brittle fracture, there is a competing fracture mechanism that links dislocations and crack nucleation to subsequent failure.

It is therefore essential that when the mechanical properties of a ceramic material are listed, some details of the microstructure are also provided. As you can see from Figure 16.3 the measured value of a mechanical property may be affected by the test method. This is particularly true in the case of hardness.

High-performance structural ceramics combine the traditional advantages of ceramics (chemical inertness, high-temperature capabilities, and hardness) with the ability to carry a significant tensile stress. The majority of the high-performance ceramics are based on silicon nitride, silicon carbide, zirconia, or alumina. Structural ceramics come in many forms—monoliths, composites, coatings, fibers, and whiskers.

16.2 TYPES OF TESTING

Ideally, before we use a ceramic in a load-bearing application we would like to have the following information about it:

- Young's modulus
- Average strength and Weibull modulus
- Toughness
- Crack propagation rate
- Cyclic fatigue resistance
- Creep curves
- Stress rupture data

We would also like to know these parameters as a function of temperature, in particular, over the temperature range at which our ceramic component is going to be used. Many different types of tests are used to obtain the mechanical properties of ceramics. There are major differences between how metals are tested compared to ceramics:

- It is often difficult to do tension tests on ceramics because of the possibility of introducing flaws.
- Ceramics are stronger in compression than they are in tension because of how cracks propagate.
- For ceramics, we need to be concerned with statistics because we don not know where the largest flaws are.

Because some mechanical properties depend on how the material was tested, it is important and necessary to establish specified test methods. Standard test methods have been adopted for ceramics. In the United States ASTM International (originally the American Society for Testing and Materials, ASTM) is the primary organization developing standards for materials testing. ASTM Committee C-28 on Advanced Ceramics has completed several standards and ones related to mechanical properties and testing are listed in Table 16.1. Specialized subcommittees work on specific areas within the field of advanced ceramics. Committee C28.01 is involved with standards related to mechanical properties and performance of monolithic ceramics. Committee C28.02 deals with reliability issues. The National Institute of Standards and Technology (NIST) has established several free databases that list mechanical properties of ceramics.

TABLE 16.1 ASTM Standards on Mechanical Properties and Testing of Ceramics

	Mechanical properties and performance
C1161-02	Test Method for Flexural Strength of Advanced Ceramics at Ambient Temperature[a]
C1198-01	Test Method for Dynamic Young's Modulus, Shear Modulus, and Poisson's Ratio for Advanced Ceramics by Sonic Resonance
C1211-02	Test Method for Flexural Strength of Advanced Ceramics at Elevated Temperatures
C1259-01	Test Method for Dynamic Young's Modulus, Shear Modulus, and Poisson's Ratio for Advanced Ceramics by Impulse Excitation of Vibration
C1273-95	Test Method for Tensile Strength of Monolithic Advanced Ceramics at Ambient Temperature
C1291-95	Test Method for Elevated Temperature Tensile Creep Strain, Creep Strain Rate, and Creep Time-to-Failure for Advanced Monolithic Ceramics
C1326-99	Test Method for Knoop Indentation Hardness of Advanced Ceramics
C1327-97	Test Method for Vickers Indentation Hardness of Advanced Ceramics
C1361-01	Practice for Constant-Amplitude, Axial, Tension-Tension Cyclic Fatigue of Advanced Ceramics at Ambient Temperature
C1366-97	Test Method for Tensile Strength of Monolithic Advanced Ceramics at Elevated Temperatures
C1368-01	Test Method for Determination of Slow Crack Growth Parameters of Advanced Ceramics by Constant Stress-Rate Flexural Testing at Ambient Temperature
C1421-01	Test Method for the Determination of Fracture Toughness of Advanced Ceramics
C1424-99	Test Method for Compressive Strength of Monolithic Advanced Ceramics at Ambient Temperatures
C1465-00	Test Method for Determination of Slow Crack Growth Parameters of Advanced Ceramics by Constant Stress-Rate Flexural Testing at Elevated Temperature
C1499-02	Test Method for Monotonic Equi-biaxial Flexural Strength Testing of Advanced Ceramics at Ambient Temperature
C1525-02	Test Method for Determination of Thermal Shock Resistance for Advanced Ceramics by Water Quenching
	Reliability
C1175-99	Guide to Test Methods for Nondestructive Testing of Advanced Ceramics
C1212-98	Practice of Fabricating Ceramic Reference Specimens Containing Seeded Voids
C1239-95	Practice for Reporting Uniaxial Strength Data and Estimating Weibull Distribution Parameters for Advanced Ceramics
C1322-02	Practice for Fractography and Characterization of Fracture Origins in Advanced Ceramics
C1336-96	Practice for Fabricating Non-Oxide Ceramic Reference Specimens Containing Seeded Inclusions
C1495-01	Test Method for Effect of Surface Grinding on Flexure Strength of Advanced Ceramics

[a]Standards for both three-point and four-point bending; –••, year of current version of standard, e.g., –01 is 2001.

16.3 ELASTIC CONSTANTS AND OTHER "CONSTANTS"

In this section we will define some of the parameters that describe the mechanical behavior of materials. Some of these parameters are constants, like Young's modulus E. Some, like hardness, are not. Hardness depends on how the material was tested.

Table 16.2 lists four elastic constants for different ceramics. These are the four that are most common.

1. E (or Y, but be careful because Y is also used in our expression for stress intensity factor)—Young's modulus (also referred to as the elastic modulus) is a material constant defined by Eq. 16.1 for a linear elastic material under uniaxial tensile or compressive stress.

$$\sigma = E\varepsilon \tag{16.1}$$

It is therefore the slope of a σ–ε curve where only elastic deformation occurs.

2. ν—Poisson's ratio is the negative ratio of the transverse strain (ε_T) to longitudinal strain (ε_L).

$$\nu = -\varepsilon_T/\varepsilon_L \tag{16.2}$$

For many ceramics and glasses it is in the range 0.18–0.30.

3. μ—Shear modulus is the ratio of shear stress to shear strain.

$$\mu = \tau/\gamma \tag{16.3}$$

4. B—Bulk modulus is the ratio of stress to strain for hydrostatic compression.

$$B = -P(\Delta V/V) \tag{16.4}$$

Although these constants are related directly to bonding forces between atoms, in real ceramics they are affected by microstructure, e.g., porosity and the presence of second phases. Because strain is dimensionless, elastic moduli have the same dimensions as those of stress: force per unit area (N/m^2) or in the SI classification Pa.

Some texts use a pair of related elastic constants λ and μ. These are known as the Lamé constants. We already

TABLE 16.2 Elastic Constants of Selected Polycrystalline Ceramics (20°C)

Material	*Crystal type*	*μ (GPa)*	B *(GPa)*	*ν*	*E (GPa)*
Carbides					
C	Cubic	468	416	0.092	1022
SiC	Cubic	170	210	0.181	402
TaC	Cubic	118	217	0.270	300
TiC	Cubic	182	242	0.199	437
ZrC	Cubic	170	223	0.196	407
Oxides					
Al_2O_3	Trigonal	163	251	0.233	402
$Al_2O_3 \cdot MgO$	Cubic	107	195	0.268	271
$BaO \cdot TiO_2$	Tetragonal	67	177	0.332	178
BeO	Tetragonal	165	224	0.204	397
CoO	Cubic	70	185	0.332	186
$FeO \cdot Fe_2O_3$	Cubic	91	162	0.263	230
Fe_2O_3	Trigonal	93	98	0.140	212
MgO	Cubic	128	154	0.175	300
$2MgO \cdot SiO_2$	Orthorhombic	81	128	0.239	201
MnO	Cubic	66	154	0.313	173
SrO	Cubic	59	82	0.210	143
$SrO \cdot TiO_2$	Cubic	266	183	0.010	538
TiO_2	Tetragonal	113	206	0.268	287
UO_2	Cubic	87	212	0.319	230
ZnO	Hexagonal	45	143	0.358	122
ZrO_2–$12Y_2O_3$	Cubic	89	204	0.310	233
SiO_2	Trigonal	44	38	0.082	95
Chalcogenides					
CdS	Hexagonal	15	59	0.38	42
PbS	Cubic	33	62	0.27	84
ZnS	Cubic	33	78	0.31	87
PbTe	Cubic	22	41	0.27	56
Fluorides					
BaF_2	Cubic	25	57	0.31	65
CaF_2	Cubic	42	88	0.29	108
SrF_2	Cubic	35	70	0.29	90
LiF	Cubic	48	67	0.21	116
NaF	Cubic	31	49	0.24	77
Other halides					
CsBr	Cubic	8.8	16	0.26	23
CsCl	Cubic	10	18	0.27	25
CsI	Cubic	7.1	13	0.27	18
KCl	Cubic	10	18	0.27	25
NaBr	Cubic	11	19	0.26	28
NaCl	Cubic	15	25	0.25	38
NaI	Cubic	8.5	15	0.27	20
RbCl	Cubic	7.5	16	0.29	21

Note: All values were calculated from single-crystal data.

defined μ, so only λ is new. The expressions that relate elastic moduli are given in Table 16.3.

$\boldsymbol{K_I}$—Stress intensity factor is a combination of flaw size, c, and applied stress, σ.

$$K_1 = \sigma Y \sqrt{c} \tag{16.5}$$

Y in Eq. 16.5 is a dimensionless parameter that depends on the crack and loading geometries. For a simple interior crack of length $2c$ and tensile loading $Y = \sqrt{\pi}$ (this is the original geometry considered by Griffith); for a surface crack under similar loading $Y = \sqrt{\pi/2}$). The units of K_I are $MPa \cdot m^{1/2}$.

The subscript refers to the type of loading geometry. There are three fundamental deformation modes that can be important for crack propagation. These modes are illustrated in Figure 16.6.

- Mode 1 opening. This is the most important for crack propagation in brittle solids. It can be achieved by an applied uniaxial tension.

TABLE 16.3 Expressions for Various Isotropic Elastic Moduli; Various Pairs of Moduli

	Independent pair of moduli			
Moduli	$\mathcal{E}$, μ	B, μ	B, ν	λ, μ
$\mathcal{E}$	$\mathcal{E}$	$9B\mu/(3B+\mu)$	$3B(1-2\nu)$	$\mu(3\lambda+2\mu)/(\lambda+\mu)$
μ	μ	μ	$3B(1-2\nu)/2(1+\nu)$	μ
B	$\mathcal{E}\mu/3(3\mu-\mathcal{E})$	B	B	$\lambda+(2\mu/3)$
ν	$(\mathcal{E}/2\mu)-1$	$(3B-2\mu)/(6B+2\mu)$	ν	$\lambda/(2\lambda+\mu)$
λ	$(\mathcal{E}-2\mu)\mu/(3\mu-\mathcal{E})$	$B-(2\mu/3)$	$3\nu B(1+\nu)$	λ

- Mode 2 sliding
- Mode 3 tearing

K_{Ic}—Critical stress intensity factor or fracture toughness. Fracture of a material in tension occurs when $K_I \geq K_{Ic}$.

H—Hardness. There are different types of hardness. Why? Because the value of a material's hardness depends on how it is tested. The hardness of a material is its resistance to the formation of a permanent surface impression by an indenter. You will also see it defined as resistance of a material to deformation, scratching, and erosion. So the geometry of the indenter tip and the crystal orientation (and therefore the microstructure) will affect the hardness. In ceramics, there tends to be wide variations in hardness because it involves plastic deformation and cracking. Table 16.4 lists hardness values on the Mohs' hardness scale, a scratch test that can be used to compare hardness of different minerals. For example, quartz has a Mohs' hardness of 7, which made flint (a cryptocrystalline quartz) particularly useful in prehistoric times for shaping bone (the mineral component is apatite with hardness 5) and shell (the mineral component is calcite with hardness 3). Mohs' hardness scale was not the first scratch hardness technique. As long ago as 1690, Christian Huygens, the famous astronomer, had noticed anisotropy in scratch hardness.

Brittleness—Although not widely used, the brittleness index (BI) has been used to quantify the brittleness of a ceramic where BI = H/K_{Ic}.

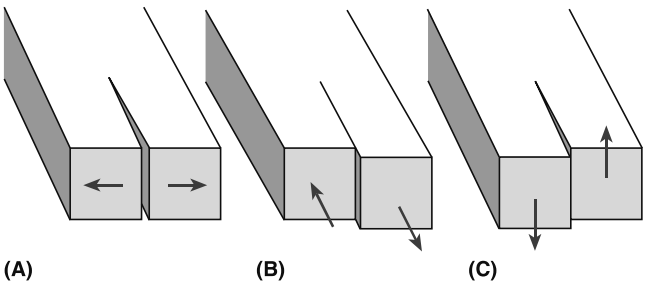

FIGURE 16.6 The three deformation modes for fracture: (a) Mode I opening. (b) Mode II sliding (in-plane shearing). (c) Mode III tearing (antiplane shearing).

16.4 EFFECT OF MICROSTRUCTURE ON ELASTIC MODULI

In Chapter 4 we showed that Young's modulus is a property that is directly related to the bonding forces between atoms. We also showed that it varies as a function of temperature. In real ceramics we have to consider the fact that we often have more than one phase present. The overall modulus is then going to be a combination of the properties of each of the phases; it lies somewhere between the high- and low-modulus components.

Analytical expressions that represent the upper and lower bounds for Young's modulus include the following.

Voigt Model

Assumption: Strain in each constituent is the same. It represents the upper bound of Young's modulus.

$$\mathcal{E} = V_2\mathcal{E}_2 + (1 - V_2)\,\mathcal{E}_1 \tag{16.6}$$

TABLE 16.4 Mohs' Hardness

Hardness number	*Mohs' scale*	*Ridgeway's extension of Mohs' scale*	*Knoop hardness expanded scale*
1	Talc	Talc	
2	Gypsum	Gypsum	32
3	Calcite	Calcite	135
4	Fluorite	Fluorite	163
5	Apatite	Apatite	430
6	Orthoclase	Orthoclase	560
7	Quartz	Vitreous silica	—
8	Topaz	Quartz or stellite	820
9	Corundum	Topaz	1340
10	Diamond	Garnet	1360
11		Fused zirconia	—
12		Fused alumina	2100
13		Silicon carbide	2480
14		Boron carbide	2750
15		Diamond	7000

TABLE 16.5 Relations between Porosity, P, and Young's Modulus, $\mathcal{E}$

$\mathcal{E} = \mathcal{E}_0(1 - aP)$	Linear decrease in Young's modulus with porosity when P is small, $a \sim 4$
$\mathcal{E} = \mathcal{E}_0(1 - aP + bP^2)$	For a low concentration of spherical pores ($a \sim 1.9$, $b \sim 0.9$)
$\mathcal{E} = \mathcal{E}_0(1 - aP)^b$	For solid foams with very high porosity $P > 0.7$ ($a = 1$, $b = 2$)
$\mathcal{E} = \mathcal{E}_0[(1 - P)^2/1 + (a - 1)P]$	a is a shape factor with values depending on porosity: $a = 2.5$ for interconnected porosity ($1/a = 0.4$) $a = 3.3$–1.4 for porosity that resembles ribbons ($1/a = 0.3$–0.7) $a = 0.6$–1.0 for isolated pores ($1/a = 0.6$–1.0) ($1/a$ is known as the Nielson shape factor)
$\mathcal{E} = \mathcal{E}_0 \exp(-aP)$	Empirical for oxides with porosity in the range 0–40% ($a \sim 4$)

Reuss Model

Assumption: Stress in each phase is the same. It represents the lower bound of Young's modulus.

$$\frac{1}{\mathcal{E}} = \frac{V_2}{\mathcal{E}_2} + \frac{(1 - V_2)}{\mathcal{E}_1} \tag{16.7}$$

Hashin and Shtrikman (HS) developed a narrower, more useful, set of bounds using basic elasticity energy theorems. The HS bounds have been shown to be best for the bulk modulus and are given by

$$\frac{B - B_1}{B_2 - B_1} = V_2 \left[\frac{V_1 (B_2 - B_1)}{B_1 + H} \right]^{-1} \tag{16.8}$$

where $H = 4\mu_2/3$ or $H = 4\mu_1/3$. Young's moduli can be obtained from B if ν is known and reasonable fits with experimental data can be obtained as shown in Figure 16.7 for alumina-tetragonally stabilized zirconia (Al_2O_3–ZrO_2) composites.

If the second phase is porosity, as is often the case in polycrystalline ceramics, then intuitively we realize that there will be a decrease in the elastic modulus. A pore has zero stiffness. Several relationships have been developed to account for the change in Young's modulus with porosity, P. These are shown in Table 16.5 where the "constants" a and b are often empirically determined; E_0 is the Young's modulus of the dense material.

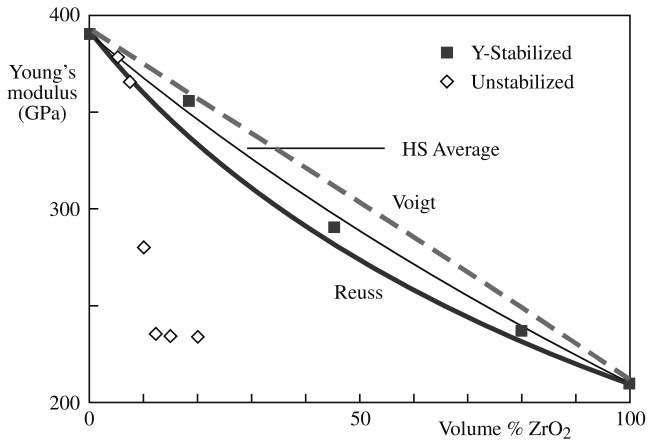

FIGURE 16.7 Comparison of predicted values of Young's modulus for an Al_2O_3 tetragonally stabilized ZrO_2 composite with experimental data.

16.5 TEST TEMPERATURE

Mechanical properties often show strong variations with temperature. We already considered in Chapter 4 how temperature affects Young's modulus. For some mechanical properties the change with temperature may be more abrupt than the gradual decrease in $\mathcal{E}$ with increasing temperature. The ductile-to-brittle transition, which occurs with decreasing temperature, is an important topic in metals. The significance of this phenomenon really came to light during World War II when there were reports of serious fractures in some of the Liberty ships (mass-produced vessels of predominantly welded construction). One of the most striking instances of this type of fracture was the T2 tanker *S.S. Schenectady* built in Portland, Oregon, which suddenly broke into two sections at 10.30 PM on January 16, 1943. The reason was that the steel alloy used to construct the hull had undergone a ductile-to-brittle transition at a temperature of 4°C. This event gave particular impetus to the study of fracture in brittle materials.

Do ceramics experience a ductile-to-brittle (or the converse) transition and is it important? Ceramics can exhibit both types of behavior over different temperature ranges. Figure 16.8 illustrates the temperature dependence of strength for ceramics.

- Region A: the fracture is brittle and the fracture strain is $\sim 10^{-3}$. There is no significant plastic deformation prior to failure and the strength varies little with temperature.
- Region B: the fracture is again brittle but slight plastic deformation occurs prior to failure. The failure strain is usually in the region 10^{-3}–10^{-2} and strength falls with increasing temperature.
- Region C: Appreciable plastic flow occurs, with strains of the order of 10^{-1} prior to failure. This behavior is rarely observed in ceramics, even in ductile polycrystalline ceramics.

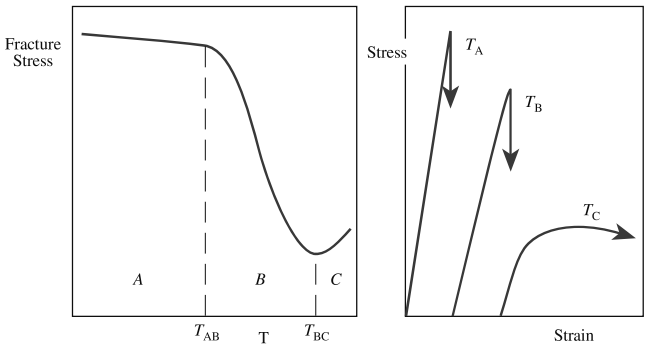

FIGURE 16.8 Illustration of the effect of temperature on fracture stress for a ceramic. The key temperatures are T_{AB} and T_{BC}.

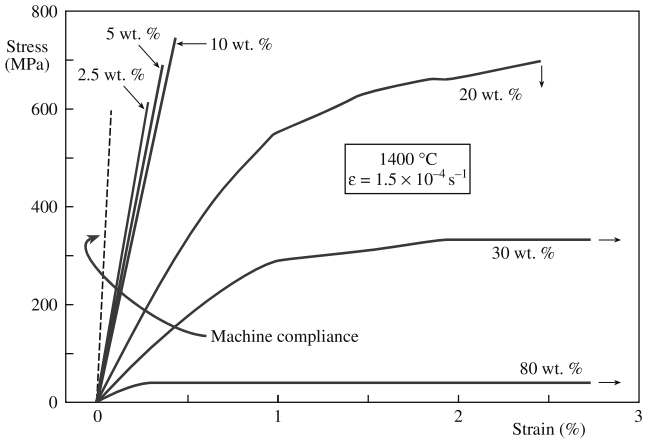

FIGURE 16.9 Stress–strain curve for Si_3N_4 at 1400°C for various amounts of silica. The machine compliance is the inherent displacement within the instrument.

The critical temperatures, T_{AB} and T_{BC}, vary greatly for different ceramics. For polycrystalline MgO the brittle-to-ductile transition occurs at ~1700°C (0.6 T_m). There is no plastic deformation in β-SiC below 2000°C. Talc, MoS_2, and graphite all deform at room temperature. MoS_2 and graphite are widely used as solid lubricants.

The transition can be important in structural ceramics (particularly nonoxides like silicon nitride) when they are used in high-temperature applications. Densification in these ceramics is often achieved using a second phase that forms a glass at grain boundaries and triple points. At temperatures near the glass softening temperature very extensive plastic flow occurs. Figure 16.9 shows σ–ε curves for silicon nitride at 1400°C containing different amounts of silica. For silica contents >20 wt% macroscopic plastic deformation occurs. At high silica contents it is believed that the glassy phase is no longer constrained at the triple points.

16.6 TEST ENVIRONMENT

In some cases the environment to which the ceramic is exposed is a very important consideration. For example, you will often see that mechanical tests on bioceramics are performed either *in vivo* or *in vitro*. Tests performed in the body are referred to as *in vivo*. Tests performed outside the body, often in conditions that seek to replicate or approximate the physiological environment, are referred to as *in vitro*. ISO Standard 6474 for alumina bioceramics specifies a bend strength >450 MPa after testing in Ringer's solution. Ringer's solution is a model liquid that resembles human body fluid.

RINGER'S SOLUTION (PARTS BY VOLUME)	
NaCl solution 0.9%	94
KCl solution 1.15%	4
$CaCl_2$ solution 1.22%	3
KH_2PO_4 solution 2.11%	1
$MgSO_4$ solution 3.82%	1
$NaHCO_3$ solution 1.3%	14
$NaHPO_4$ solution 1 M	13

RULE OF THUMB

Compressive fracture strength is 10–15 times greater than tensile fracture strength.

16.7 TESTING IN COMPRESSION AND TENSION

The tensile test is the most frequently used procedure to determine the tensile strength of a metal. However, it is not used as widely for ceramics because of their inherent brittleness. It is difficult to make the typical "dog-bone"-shaped samples, where the cross-sectional area is reduced in the gage length. We could do this with a ceramic, but the machining needed to give this shape is likely to introduce surface flaws. In many tensile test instruments the sample under test is connected by means of a screw thread. This is often tricky to machine with a ceramic and it may also break in the grips. Finally, because ceramics fail after only about 0.1% strain, the specimens under test must be perfectly aligned or bending stresses will be introduced, which will complicate things.

In some practical situations we require ceramics to support a tensile load. Consider the growth of silicon single crystals by the Czochralski process, which involves pulling the crystal from the melt. The crystal is supported entirely by a narrow region called the neck, about 3 mm in diameter. It is possible to support a total crystal weight of about 200 kg. This requirement determines the maximum overall volume of a silicon boule. The diameter is controlled by our ability to produce dislocation-free crystals as described in Chapter 29. Steel-reinforced concrete and safety glass are two exam-

TABLE 16.6 Ratio of Compressive Strength σ_{cc} to Bending Strength, σ_c

Ceramic	*Grain size (μm)*	σ_{cc}/σ_c
TiB_2	20–50	4–6
ZrB_2	20–50	4–6
B_4C	1	7
WC	1–6	4–6
Al_2O_3	1–100	4–30
$MgAl_2O_4$	1	7
ThO_2	4–60	13–17
UO_2	20–50	5–18

ples in which a ceramic is prestressed in compression to increase its ability to support a tensile load.

Stress–strain curves for metals look very similar and provide similar results whether the testing is carried out in tension or compression. Ceramics are generally stronger in compression and can tolerate high compressive loads. Some examples are given in Table 16.6. However, reliable compressive strength data are limited for ceramics. Note that the Young's modulus will be the same because the curves will have the same slope.

One ceramic that is widely tested in compression is concrete. Concrete is a ceramic-matrix composite consisting of a mixture of stone and sand (called the aggregate) in a cement matrix. The aggregate provides the strength and the cement provides the workability. When concrete is used in construction it must always be loaded in compression. As shown in Figure 16.10 cracks behave differently in compression than they do in tension. In compression, cracks twist out of their original orientation and propagate stably along the compression axis. The result is that the sample will crush rather than fracture. Fracture is not caused by rapid unstable crack propagation as it is in tension.

In tension we are concerned with the largest crack, the "critical flaw," particularly if it is on the surface. In compression we are concerned with the average flaw size, c_{av}. We can estimate the compressive stress to failure by substituting c_{av} into Eq. 16.5 and using a multiplier between 10 and 15. Teeth are ceramic composites: they survive for years even when many cracks are present.

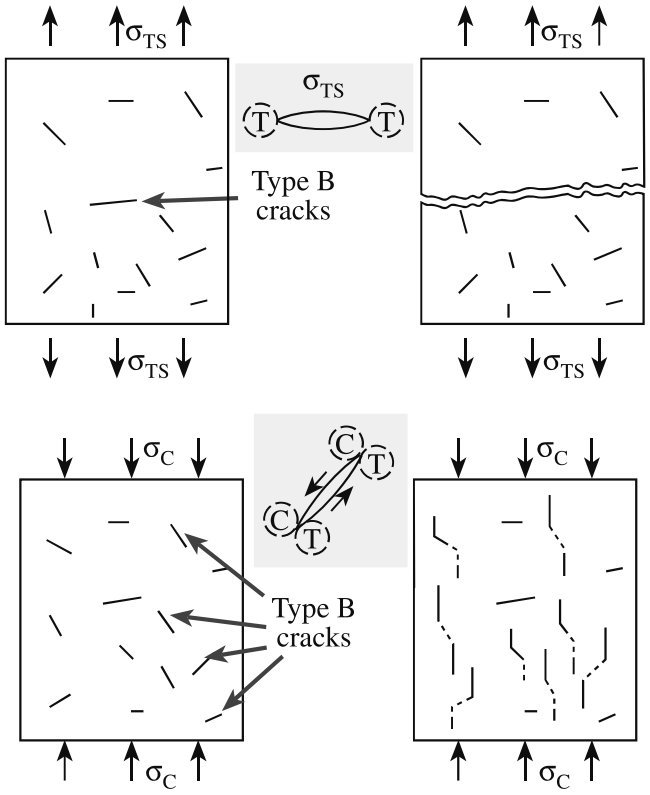

FIGURE 16.10 Illustration of unstable and stable crack propagation for a brittle material in tension (T) and compression (C), respectively. Stable crack propagation will lead to crushing.

16.8 THREE- AND FOUR-POINT BENDING

To avoid the high expense and difficulties of performing tensile tests on ceramics, tensile strength is often determined by the bend test. There are two geometries and these are illustrated in Figure 16.11. The main advantage of the bend test, other than its lower cost, is that we use simple sample geometries. The specimens have either a rectangular or cylindrical geometry. The four-point bend test is preferred because an extended region with constant bending moment exists between the inner rollers.

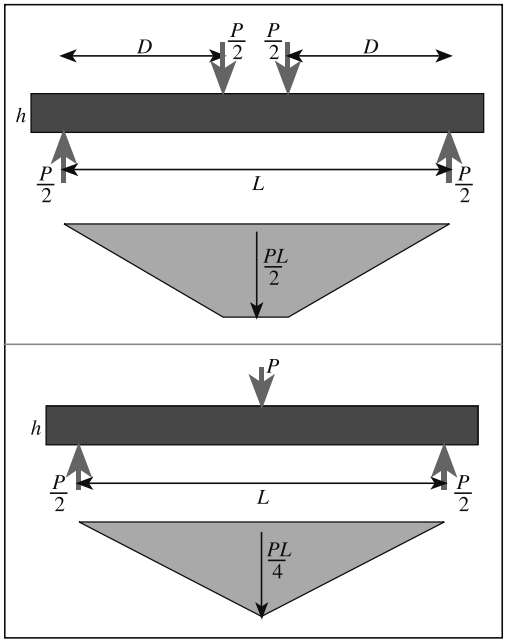

FIGURE 16.11 The geometries for three- and four-point bending.

The maximum tensile stress in the surface of the beam when it breaks is called the modulus of rupture (MOR), σ_r. For an elastic beam it is related to the maximum moment in the beam, M

MODULUS OR RUPTURE EQUATIONS

Three-point bend: $\sigma_r = \dfrac{3PL}{2BW^2}$

Four-point bend: $\sigma_r = \dfrac{3PD}{BW^2}$

$$\sigma_r = \frac{6M_r}{BW^2} \qquad (16.9)$$

W is the height of the beam and B is its thickness. For the case of bend testing a ceramic this equation is applicable only when the distance between the inner rollers is much greater than the specimen height.

Other terms are also used including flexural strength, fracture strength, and bend strength. The bend test is also known as a flexure test and the resistance of a beam to bending is known as its flexural rigidity. The terminology can be a little confusing, but this test is important because it is widely used and probably the best studied strength test for ceramics.

SENB AND CN SPECIMENS

Typical dimensions:

$B = 3\,\text{mm}$, $W = 4\,\text{mm}$

$S_2 = 20\,\text{mm}$, $S_1 = 40\,\text{mm}$

Crack depth $c/W \sim 0.5$
Total specimen length 50 mm

Examples of data from such tests are shown in Figure 16.12 for polycrystalline alumina. The main comment that can be made is that there is a wide variation in the values! Grain size differences between the samples are clearly one of the factors contributing to this variation.

The main disadvantage of the bend test is that the stress distributions can be complex and nonuniform. The consequence is that under certain conditions, particularly when the largest flaws in the sample are located in the interior of the specimen, the strength of the ceramic will be overestimated.

16.9 K_{Ic} FROM BEND TEST

There are several techniques to determine K_{Ic} for a ceramic. The two main approaches are to use indentation or bending. In the bend test a notch is introduced, usually using a diamond-tipped copper cutting wheel, into the tensile side of the specimen as shown in Figure 16.13. In Figure 16.13a the

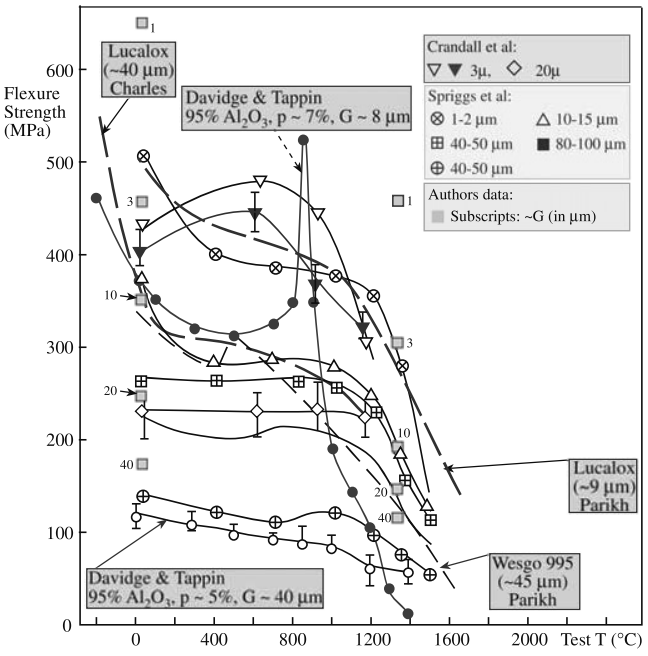

FIGURE 16.12 Flexural strength of polycrystalline Al_2O_3 as a function of test temperature.

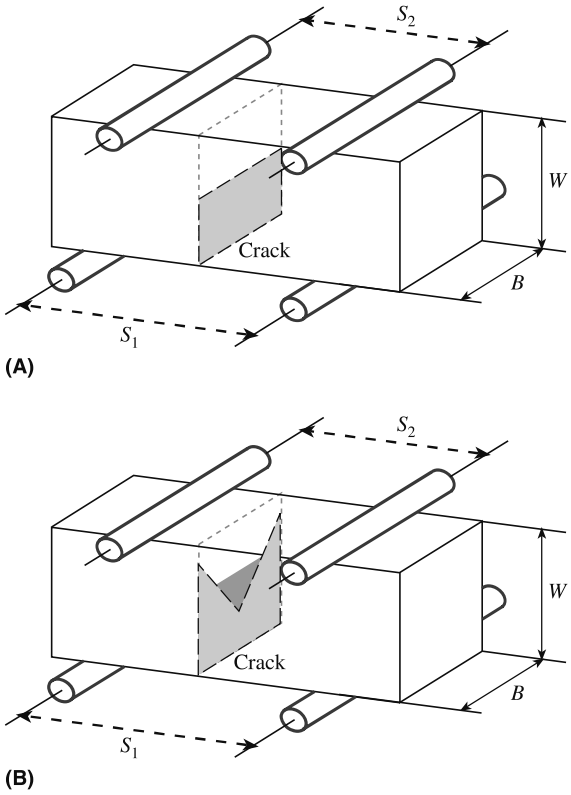

FIGURE 16.13 Geometries for (a) SENB and (b) CN specimens used to determine K_{Ic}.

notch is flat (single-edged notched beam, SENB), whereas in Figure 16.13b it is chevron-shaped. The specimen is loaded, usually in four-point bend, until it fails at F_{Max} and K_{Ic} is calculated.

For the SENB

$$K_{Ic} = \frac{3\sqrt{c}\,(S_1 - S_2)\xi F_{Max}}{2BW^2} \qquad (16.10)$$

c is the length of the initial crack that we introduced and ξ is a calibration factor. The advantage of the SENB test is that it is quite simple, although it tends to overestimate K_{Ic} because the crack is often not atomically sharp. For ceramics having very fine grain sizes the notch must be very narrow.

For the chevron notched (CN) specimen

$$K_{Ic} = \frac{(S_1 - S_2)\xi^* F_{Max}}{BW^{3/2}} \qquad (16.11)$$

where ξ^* is a compliance function. Sometimes you will see Eq. 16.11 written in such a way that all the geometric terms are grouped together as a single geometric function Y^*. Then we have

$$K_{Ic} = \frac{F_{Max}}{B\sqrt{W}} Y^* \qquad (16.12)$$

The value of Y^* is then necessary for different specimen geometries and different notch geometries. Two approaches can be used to obtain Y^* (see Specific References).

CAUTION

Fracture toughness values for different ceramics may depend on technique used to measure them.

The advantage of the CN geometry is that we do not need to worry about introducing a sharp precrack. Our original notch is made by two saw cuts to produce a triangularly shaped cross section. A crack is easily initiated at the tip of the chevron, but the increasing cross section of the crack front causes crack growth to be stable prior to failure. Further crack extension requires an increase in the applied load and it is possible to create an atomically sharp crack before the specimen fails. Also you can see from Eq. 16.11 that we do not need to know the actual crack length. In fact, we do not need to know any of the materials properties.

16.10 INDENTATION

Measuring the hardness of a ceramic is important and this is usually done using an indentation test. The basic idea is that a permanent surface impression is formed in the material by an indenter. We then measure the actual or projected area of the impression. The hardness is then determined by dividing the applied force, F, by this area. The processes that happen under the indenter tip can be quite complex. We often see a deviation from what is called "Hertzian" behavior where the indentation stress is proportional to the indentation strain (Figure 16.14). The deviation is due to plasticity beneath the indenter as illustrated in Figure 16.15. We discuss this more in Chapter 17. Cracking can also occur on indenting and this can be used as a means of determining fracture toughness.

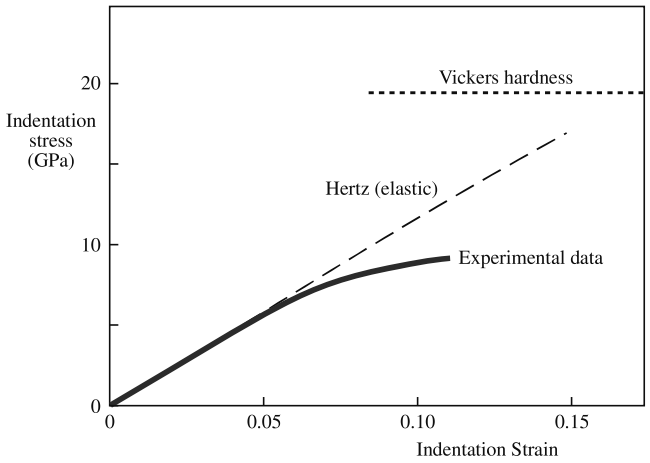

FIGURE 16.14 Indentation stress versus indentation strain.

There are many different hardness tests and each gives a different number. The common hardness tests are listed in Table 16.7 and the geometries of the impression are shown in Figure 16.16. It is possible to convert between different hardness scales, but the conversion depends on both the material and its microstructure. The most reliable data are for steels because most of the work has been done on these alloys. Detailed conversion tables for metals and alloys are available in ASTM Standard E 140, "Standard Hardness Conversion Tables for Metals." There are different regimes of hardness based on the load used as shown in Table 16.8. These divisions are somewhat arbitrary, but they are commonly accepted.

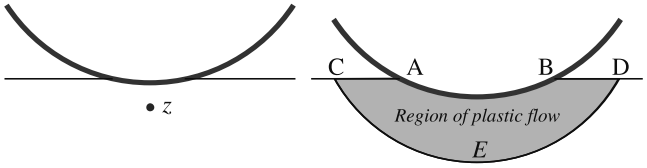

FIGURE 16.15 Plasticity under the indenter (the shaded area) causes the deviation from Hertzian behavior.

TABLE 16.7 Details of Common Hardness Tests

Test	*Indenter*	*Description*	*Equation*	*Notes*
Brinell	Hardened steel ball	Brinell hardness number (BHN) is applied force divided by surface area of indentation	BHN = $F/\pi Dt$	Spherical indenters not used for ceramics
		Meyer hardness number (MHN) uses projected area	MHN = $4F/\pi d^2$	
Vickers	Square pyramid	Vickers hardness number (VHN) using contact area	VHN = $1.854F/a^2$	The ceramics community uses mainly the number calculated using the projected area; need to be careful when comparing data from different sources
		VHN using projected area	VHN = $2.000F/a^2$	
Knoop	Elongated pyramid	Knoop hardness number (KHN)	KHN = $14.2F/L^2$	
Rockwell	Various indenter types/loads	Dimensionless number and various hardness scales		Widely used for metals but not often for ceramics except cemented carbides

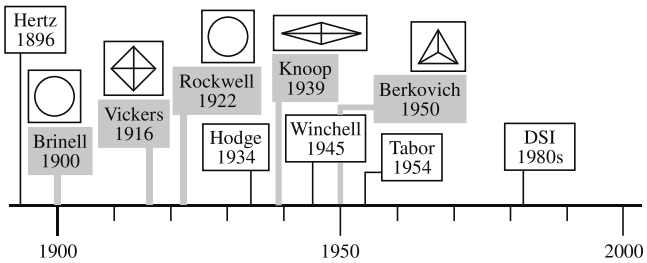

FIGURE 16.16 The evolution of common hardness tests and the corresponding indenter shapes.

TABLE 16.8 Hardness Regimes

Regime	*Applied load (N)*	*Comments*
Microhardness	0.0098–1.96	Hardness value decreases as load increases Possibility for very large variations in values depending on technique used and microstructure Surface effects may dominate
Low load hardness	1.96–98.1	
Standard hardness	>98.1	Hardness independent of applied load and microstructure.

16.11 FRACTURE TOUGHNESS FROM INDENTATION

We can obtain the fracture toughness from indentation tests. The basic idea is illustrated in Figure 16.17. We get an indent and radial cracks. The hardness is then

$$H = P/\alpha a^2 \tag{16.13}$$

α is a numerical factor that depends on the shape of the indenter. For a Vickers indenter $\alpha = 2$. P is the load in newtons.

The critical stress intensity factor is obtained by assuming that the applied stress intensity caused by the load is equal to the critical stress intensity for crack propagation.

$$K_{Ic} = \frac{\zeta(\mathcal{E}/H)^{\frac{1}{2}} P}{c^{\frac{3}{2}}} \tag{16.14}$$

ζ is a dimensionless constant, which for ceramics has an average value of 0.016 ± 0.004. The use of indentation techniques for determining K_{Ic} has been the subject of many studies since being introduced by Lawn and Wilshaw (1975). The most commonly used variant, termed the indirect method, uses indentation followed by determination of the strength after indentation using bend testing. The main concern is to ensure that the crack does not grow between indentation and bend testing. To minimize effects

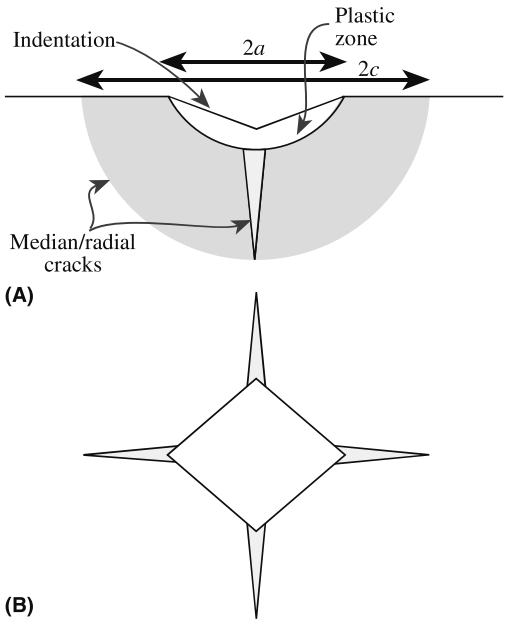

FIGURE 16.17 Cracks at an indent allow determination of K_{Ic}.

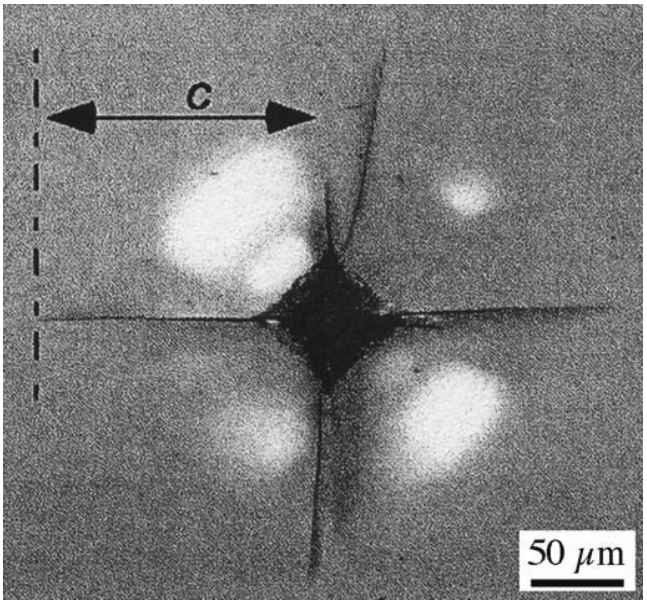

(C)

FIGURE 16.17 *Continued*

of reactive species such as water a drop of oil may be placed on the indent. Tests seem to give reproducible values for K_{Ic}.

16.12 NANOINDENTATION

The nanoindentation technique was developed in the 1980s because of the need to determine the mechanical properties of thin films and surfaces that had been modified, for example, by ion implantation. To avoid the influence of the substrate the penetration depth of the indenter must be less than 10% of the film thickness. Consequently penetration depths are on the order of nanometers rather than millimeters, which is common for conventional indentation tests.

Nanoindentation is also used to test small volumes of material. The low loads used mean that the extent of cracking is much smaller than in conventional indentation methods.

Two parameters are often of most interest in nanoindentation testing:

- Elastic modulus
- Hardness

Load (P) versus depth of penetration (h) curves, also called compliance curves, are the output from a nanoindentation test. The curves are obtained as load is applied to the indenter tip up to some maximum value and then back to zero. Figure 16.18 shows a general compliance curve for a material that undergoes both elastic and plastic deformation. When the load applied to the indenter is released the material attempts to return to its original shape. The slope of the elastic unloading region (dP/dh) can be used to determine the modulus and hardness. There are several different equations depending on the tip geometry. If the material is plastically deformed it cannot return to its original shape and there is a resi-dual impression, h_r. The magnitude of h_r will be greater for a metal such as steel than for a ceramic such as sapphire.

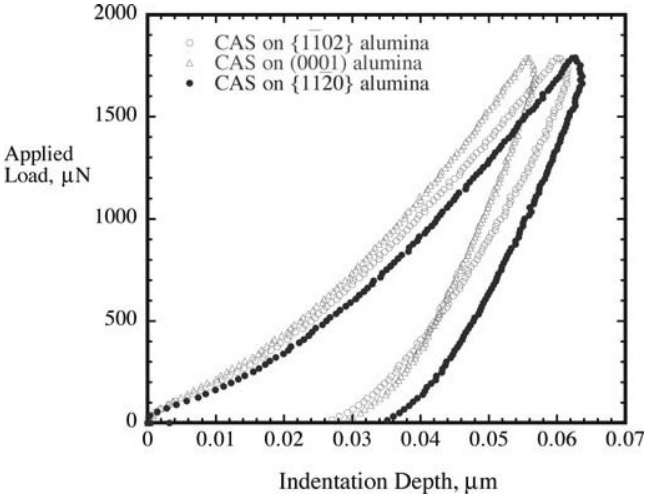

FIGURE 16.18 Load-displacement data on the 1.8 mN indentations of CAS films on three different alumina substrates.

Nanoindentation is a powerful technique because the shape of the load-displacement curve can be used to identify effects such as phase transformations, cracking, and film delamination during indentation. It is also important in studying the mechanical properties of nanomaterials, such as carbon nanotubes. There is reference now to a picoindenter, which is a combination of a nanoindenter and an atomic force microscope (AFM).

16.13 ULTRASONIC TESTING

The basic principle of this method is that the velocity of an ultrasonic wave through a material is related to its density and elastic properties. This is one example of a dynamic method for determining elastic constants, such as Young's modulus and shear modulus. Dynamic methods are more accurate than static methods with uncertainties of <0.5% (±10% would be more typical for static methods).

To determine the shear modulus and Poisson's ratio we need the velocity of the longitudinal and transverse waves, v_L and v_t. The equations are

$$\mu = \rho v_t^2 \qquad (16.15)$$

TRANSVERSE WAVE VELOCITIES

	Al_2O_3	Al
μ	163 GPa	25 GPa
ρ	3970 kg/m^3	2710 kg/m^3
v_t	6.4 km/s	3.0 km/s

$$\nu = \frac{1-2(v_t/v_L)^2}{2\left[1-(v_t/v_L)^2\right]} \qquad (16.16)$$

$$\mathcal{E} = 2\mu(1+\nu) \qquad (16.17)$$

Conversely, if we know the elastic moduli we can determine the magnitude of the sound velocities. For ceramics with high moduli and low density the sound velocities will be much higher than many metals. The propagation of sound waves through ceramics is particularly important during earthquakes. The earth's crust is composed primarily of silica and aluminosilicates. Using Eqs. 16.15 and 16.16 we can show for SiO_2, the primary constituent of rocks such as granite, that the longitudinal waves are the first shocks to arrive after an earthquake, followed by the transverse waves; $v_L = 6.04$ km/s and $v_t = 4.1$ km/s for quartz. The surface waves are the last to arrive, having a velocity <4 km/s, but these often have the most devastating effect.

Ultrasonic testing is widely used in the concrete industry to determine the presence or absence of voids, cracks, and other imperfections and to measure deterioration that might have occurred due to age or through fire or frost damage.

16.14 DESIGN AND STATISTICS

When we measure the strength of a series of equivalent ceramic specimens we typically find considerable scatter in the results. The reason is due to the size distribution of flaws that are responsible for failure. This behavior is very different from that of metals. Consequently we have to adopt different design approaches when we use ceramics.

When we design components using metals we determine the maximum stress that will be present in the component and then select a metal that has a larger strength. A reasonable safety margin is often included. This approach is referred to as deterministic design. It does not work with ceramics because of the large scatter. Rather we have to use a probabilistic approach in which we represent this scatter in a quantitative way so that these materials can be used safely. The most popular method is to use Weibull statistics, which are based on the weakest link approach. The analogy is to consider a chain the strength of which is determined by the weakest link.

The Weibull distribution function is shown in Figure 16.19 and gives the probability of survival (P_S), or, alternatively, the probability of failure (P_F), of a stressed volume V.

$$P_S = 1 - P_F = \exp\left[-\int_V \left(\frac{\sigma-\sigma_{min}}{\sigma_0}\right)^m dV\right] \qquad (16.18)$$

The Weibull distribution function contains three parameters:

m = Weibull modulus, which indicates how rapidly the strength falls as we approach σ_0.

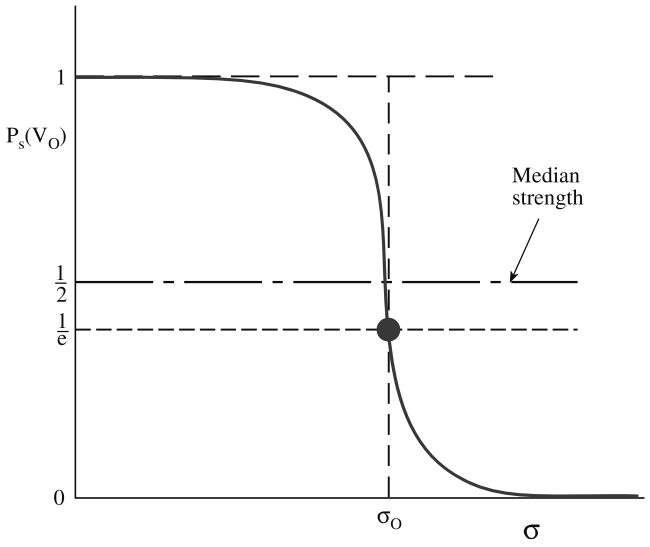

FIGURE 16.19 The Weibull distribution function.

σ_0 = the characteristic strength for which the survival probability is 0.37 ($1/e$).

σ_{min} = the stress level below which the probability of failure is zero.

Because there is always a possibility, albeit slight, of our component having a very large flaw, we usually set $\sigma_{min} = 0$. This leads to the two-parameter form that is used for ceramics.

$$P_S = \exp\left[-\int_V \left(\frac{\sigma}{\sigma_0}\right)^m dV\right] \qquad (16.19)$$

If the full volume is under uniform uniaxial tension then we can write Eq. 16.19 as

$$P_S = \exp\left[-\left(\frac{\sigma}{\sigma_0}\right)^m\right] \qquad (16.20)$$

For other geometries we need to include the loading factor L_F. This takes into account the stress distribution. For uniaxial tension $L_F = 1$; for other loading geometries see Table 16.9. The product ($L_F V$) is often termed the effective volume, V_{eff}, as it indicates how "effectively" the body is being stressed.

Taking the natural logarithm of both sides of Eq. 16.20 we get

$$\ln\left(\frac{1}{P_S}\right) = \left(\frac{\sigma}{\sigma_0}\right)^m$$

If we take natural logarithms again we get

TABLE 16.9 Examples of Loading Factors[a]

Geometry	*Loading factor,* L_F
Uniaxial tension	1
Pure bending	$1/[2(m+1)]$
Three-point bending	$1/[2(m+1)^2]$
Four-point bending	$(mL_i + L_o)/[2L_o(m+1)^2]$

[a] L_i, inner span; L_o, outer span.

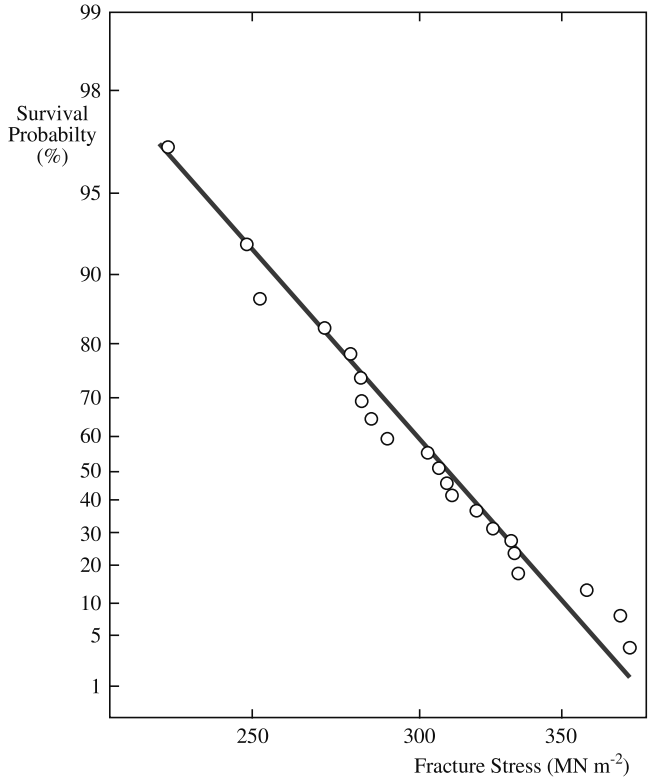

FIGURE 16.20 Weibull plot showing probability of failure as a function of fracture stress.

$$\ln\left[\ln\left(\frac{1}{P_S}\right)\right] = m\ln\left(\frac{\sigma}{\sigma_0}\right)^m = m\ln\sigma - m\ln\sigma_0$$

Now if we plot $-\ln\ln(1/P_S)$ versus $\ln\sigma$ we will get a straight line of slope $-m$ as shown in Figure 16.20. The higher the Weibull modulus the lower is the variability of strength. Values for ceramics are often in the range of 5–20 (compared, for example, to steels, which have values of about 100). Figure 16.21 shows how the Weibull modulus affects the survival probability.

The Weibull modulus, which is the parameter often of most interest, is obtained experimentally by testing a batch of samples. We need a large number of specimens to get an accurate value of m. Usually a minimum of 30 samples is required, which will typically give m within 20%. Up to 100 samples is not uncommon, which will give m with a greater than 90% confidence.

The following sequence of steps is used to determine m from a set, N, of measured strengths:

1. Rank the specimens in order of increasing strength.
2. Determine P_S. For the jth specimen this is often given as the approximation $P_S(j) = 1 - j/(N + 1)$. A more accurate expression that may be used instead is $P_S = 1 - [(j - 0.3)/(N + 0.4)]$.

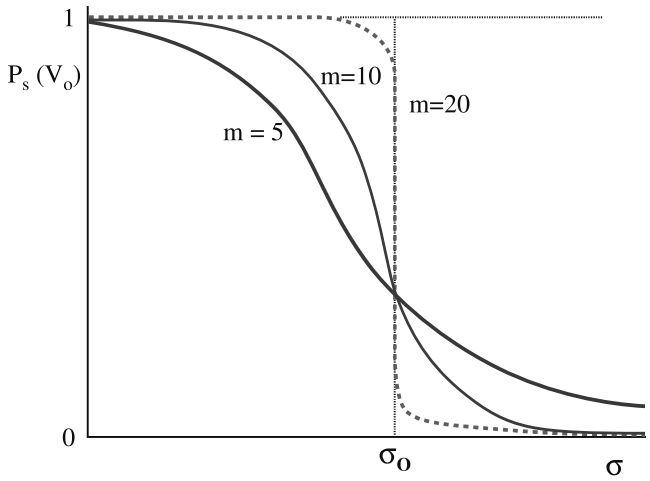

FIGURE 16.21 Illustration of the effect of m on survival probability. When m changes P_S changes.

3. A plot $-\ln\ln(1/P_S)$ versus $\ln\sigma$, the slope, which can be determined by a least-squares fit, gives m.

In ceramics there is a volume dependence of the strength. This can be illustrated quite easily using a stick of chalk. As the chalk becomes smaller it becomes stronger. The reason is again due to flaws. There is an increased probability of finding a larger flaw in a larger body as illustrated in Figure 16.22. This effect can be expressed mathematically as

$$P_S = \exp\left[-\left(\frac{V}{V_0}\right)\left(\frac{\sigma}{\sigma_0}\right)^m\right]$$

where $V = nV_0$. An example of the size effect is shown in Figure 16.23 for Si_3N_4 springs. The springs have different diameters of the wire and of the coil and different numbers of coils were measured.

STRENGTH AND VOLUME

The strength of metal samples does not depend on volume.

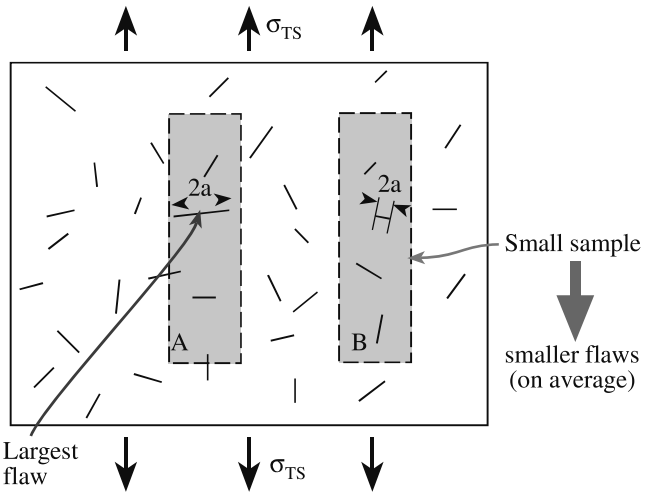

FIGURE 16.22 The largest flaw will be the weakest link and the source of failure. Smaller samples have smaller flaws.

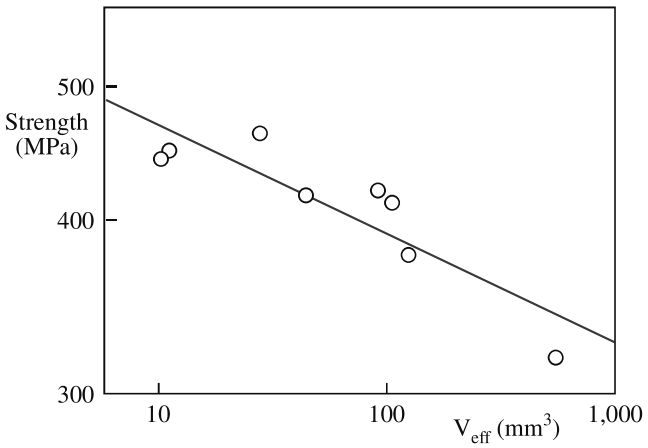

FIGURE 16.23 Fracture stress as a function of volume for Si_3N_4 springs.

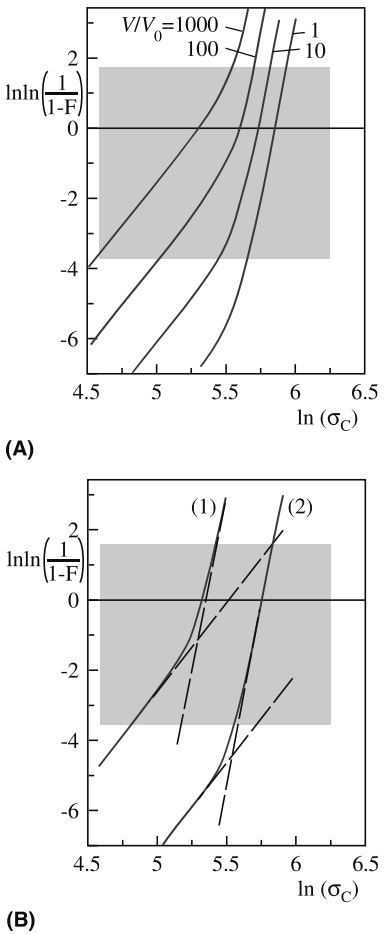

FIGURE 16.24 (a) Different flaws lead to different values of *m*. (b) Weibull plot for a sample having both surface and volume flaws.

Complications arise if we have different flaw populations, for example, we may have pores and inclusions introduced during sintering and surface flaws introduced during grinding. The different flaws may lead to different Weibull distributions and different Weibull moduli. Figure 16.24a illustrates the superposition of two flaw types and Figure 16.24b for a sample containing surface and volume flaws. And we have new equations.

For two different surface flaw types:

$$P_S = \exp\left[-\left(\frac{\sigma_c}{\sigma_1}\right)^{m_1} - \left(\frac{\sigma_c}{\sigma_2}\right)^{m_2}\right]$$

For flaw type 1 we have σ_1 and m_1; for flaw type 2 we have σ_2 and m_2.

For two different types of volume flaws:

$$P_S = \exp\left[-\frac{V_{eff1}}{V_0}\left(\frac{\sigma_c}{\sigma_{v1}}\right)^{m_1} - \frac{V_{eff2}}{V_0}\left(\frac{\sigma_c}{\sigma_{v2}}\right)^{m_2}\right]$$

As you now realize it is impossible to design a ceramic where the probability of failure is zero. Table 16.10 gives some examples of what might be considered acceptable probabilities of failure.

Proof testing can be used to truncate the extreme tail of the Weibull distribution. Components are tested up to a certain proof-test stress, σ_{PT} (Figure 16.25), for a short period of time. The weakest ones obviously fail and can be weeded out. We then have increased confidence in the remaining components. We often have to proof test stresses close to the design stress. For a ceramic with $m = 10$, reducing the risk of rupture from 0.1 to 0.05 requires that the component be proof tested to 93% of the design stress. To reduce the probability of failure by an order of magnitude, down to 0.02, the part must be proof tested to 99% of the design stress (Figure 16.26). We have a good level of confidence in the remaining components withstanding any stress < σ_{PT}.

CARES (*C*eramics *A*nalysis and *R*eliability *E*valuation of *S*tructures) is a public-domain program from the National Aeronautic and Space Agency (NASA) that incorporates Weibull statistics. The program was formally known by the less friendly acronym SCARE (*S*tructural *C*eramics *A*nalysis and *R*eliability *E*valuation).

The NASA CARES program can be found at http://www.grc.nasa.gov/WWW/LPB/cares/life/refs.html.

The following considerations and assumptions apply to the use of Weibull statistics:

TABLE 16.10 Suggested Failure Probabilities

P_F	*Possible consequences of failure*	*Example*
0.3	Slight inconvenience	Sticks of chalk
10^{-2}	Inconvenience and small expense	Ceramic cutting tool
10^{-6}	Injury	Window on a vacuum system
10^{-8}	Loss of life and significant expense	Ceramic protective tile on space shuttle

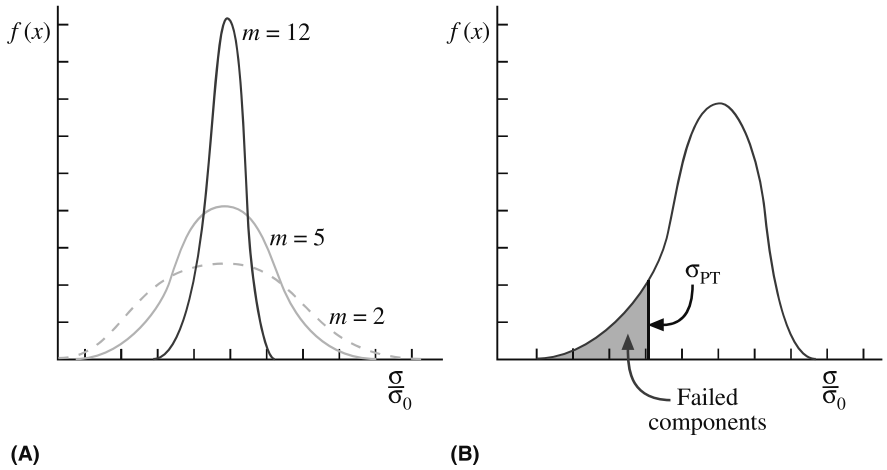

FIGURE 16.25 (a) Probability distributions for different values of *m*. (b) Proof testing up to σ_{PT} removes the weakest components from the distribution.

- There is a need to ensure that the conditions under which we are testing match those in service. For example, flaws in a component may appear during service as a result of oxidation or corrosion that might not be present in the test sample.
- There is a complex distribution of flaws.
- More than one type of flaw may be present.

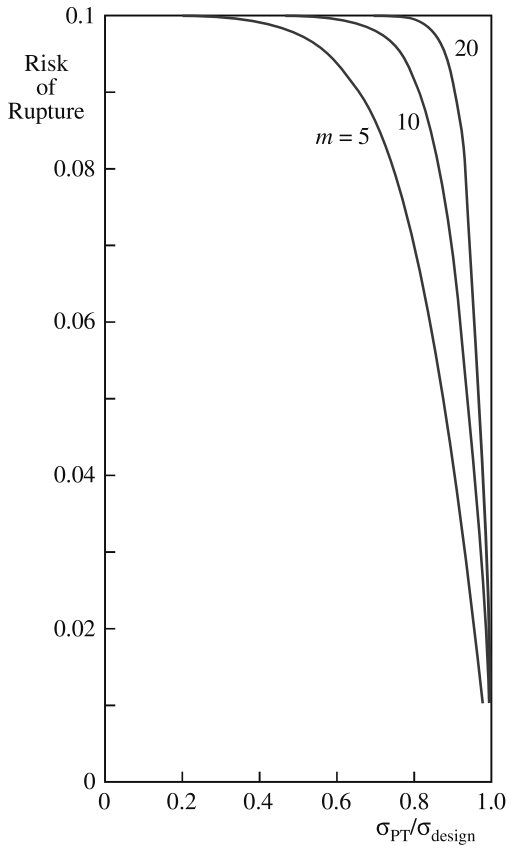

FIGURE 16.26 Plot showing the risk of rupture after proof testing to the ratio of proof-test stress to design stress.

16.15 SPT DIAGRAMS

Stress–probability–time (SPT) diagrams incorporate the time dependence of strength into failure statistics. They give lifetime predictions. An illustration of the use of SPT diagrams is in bioceramrcs.

An important requirement for any implant material is how long it will last. Because of the nature of failure of ceramic components it is not possible to provide a specific and definite lifetime for each individual implant. Rather we have to express failure in terms of probabilities. Figure 16.27 is an applied stress versus probability of time to failure (SPT) diagram for medical grade alumina. It shows that for a 30-year survival period with failure of no more than 1 in 100 components the maximum tensile stress that can be applied is limited to <200 MPa. If stresses of

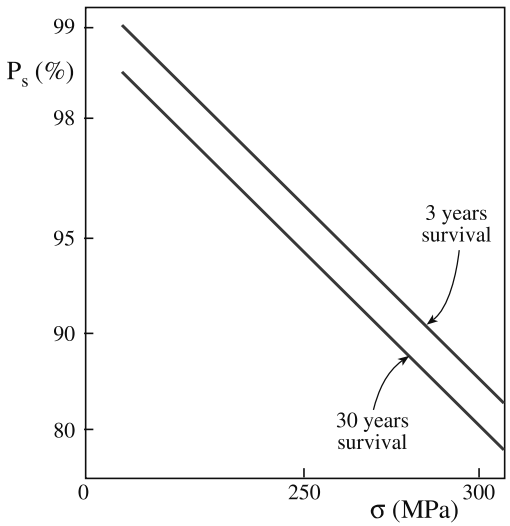

FIGURE 16.27 SPT diagram for medical grade Al_2O_3. The survival probability decreases with increasing stress and longer times.

TABLE 16.11 Average Annual Wear Rates of Articulating Surfaces in Total Hip Prosthesis

Materials	*Wear rate (μm/year)*
Co–Cr–Mo alloy/UHMWPE	200
Alumina/UHMWPE	20–130
Alumina/alumina	2

250 MPa are applied to the ceramic component, within 3 years 4% of the implants is likely to fail and by 30 years 7% will probably fail. Use of SPT diagrams such as these, together with finite element analysis of local stress distributions, makes it possible to design ceramic components that have very low probabilities of failure during the lifetime of the patient. Numerous clinical studies have been performed on patients receiving total hip replacement. One of the main problems that have been encountered is that of wear between the head (ball) and the socket. Although there is considerable variation in the data, it is generally found that the wear rate for systems with metal balls is much higher than the rate with alumina balls. And alumina balls in alumina sockets produce the least wear of any materials combination as indicated in Table 16.11.

CHAPTER SUMMARY

Flaws dominate the mechanical properties of ceramics. They determine how we test them and how we design components from them. Flaws are also the reason why ceramics are stronger in compression than tension. In this chapter we described the methods used to measure mechanical properties of ceramics. The important ones are bend testing, compression testing, and indentation. To determine the mechanical properties of small volumes we use nanoindentation. This technique is especially important for thin films, surfaces, and nanomaterials. An understanding of statistics is particularly important when using ceramics in load-bearing applications. The Weibull approach is the one most widely used for ceramics.

PEOPLE IN HISTORY

Mohs, Fredrich (1773–1839) was a German mineralogist. His original paper on the scratch test and the eponymous hardness scale was published in *Grundriss der Mineralogie* in 1822.

Poisson, Siméon Denis (1781–1840) was a French mathematician. He was more suited to mathematics than medicine because of his clumsiness. This was not an impediment for a mathematician! In 1837 he published a paper on probability, which described the Poisson distribution. During his career Poisson published more than 300 mathematical works and was reported to have said "Life is good for only two things, discovering mathematics and teaching mathematics."

Ringer, Sidney (1835–1910) was a British physician and physiologist. His original salt solution was developed in 1882 and used to prolong the survival time of tissue taken from a frog's heart. The solution used to test biomaterials differs in composition from that developed for amphibians.

Young, Thomas (1773–1829) was an English physician physicist. He could read fluently by age two and presented his first paper to the Royal Society at the young age of 20. By 1801 he was a professor at the Royal Institution in London. He was probably best known for his classic double slit experiment, which demonstrated the wave nature of light.

Weibull, E.H. Waloddi (1887–1979) was a Swedish engineer. The original paper describing his statistical analysis was published in 1939, "A Statistical Theory of the Strength of Materials," *Ingeniöersvetenskapsakademiens Handlingar* **151**, 1–45. Weibull was a frequent visitor to Wright Patterson Air Force Base in Ohio and lectured at the Air Force Institute of Technology. In 1972 he was awarded the American Society of Mechanical Engineers gold medal for his achievements. King Carl Gustav XVI of Sweden presented Weibull with the Great Gold medal from the Royal Swedish Academy of Engineering Sciences in 1978.

GENERAL REFERENCES

Cook, R.F. and Pharr, G.M. (1994) "Mechanical properties of ceramics," in *Materials Science and Technology*, edited by R.W. Cahn, P. Haasen, and E.J. Kramer, VCH, Weinheim, p. 339.

Davidge, R.W. (1979) *Mechanical Behavior of Ceramics*, Cambridge University Press, Cambridge, UK. A brief introduction.

Engineered Materials Handbook, Volume 4, *Ceramics and Glasses* (1991) ASM International (Materials Park, OH. A useful reference.

Fischer-Cripps, A.C. (2002) *Nanoindentation*, Springer, New York.

Gordon, J.E. (2002) *The New Science of Strong Materials, or Why You Don't Fall Through the Floor*, 2nd edition, Penguin, London. An excellent introduction to mechanical properties of materials; the original was published in 1968.

Green, D.J. (1998) *An Introduction to the Mechanical Properties of Ceramics*, Cambridge University Press, Cambridge, UK.
Lawn, B. and Wilshaw, T.R. (1975) "Indentation fracture—principles and applications," *J. Mater. Sci.* **10**, 1049. The paper that showed how to derive K_{Ic} from indenter experiments.
McColm, I.J. (1990) *Ceramic Hardness*, Plenum Press, New York.
Munz, D. and Fett, T. (1999) *Ceramics: Mechanical Properties, Failure Behavior, Materials Selection*, Springer, Berlin.
Richerson, D.W. (2006) *Modern Ceramic Engineering, Properties, Processing and Use in Design*, 3rd edition, Taylor & Francis, Boca Raton, FL. Chapter 18 describes design approaches for ceramics.
Sines, G. and Adams, M. (1978) "Compression testing of ceramics," in *Fracture Mechanics of Ceramics*, Vol. 3, Plenum Press, New York, p. 403.
Wachtman, J.B. (1996) *Mechanical Properties of Ceramics*, Wiley, New York.

SPECIFIC REFERENCES

Blum, J.J. (1975) "Slice synthesis of three dimensional work-of-fracture specimens," *Eng. Fract. Mech.* **7**, 593. The slice model for determining *Y**, the geometric "constant" in K_{Ic} measurements (cf. Munz *et al.*).
Hashin, Z. and Shtrikman, S. (1963) "A variational approach to the theory of the elastic behavior of multiphase materials," *J. Mech. Phys. Solids* **11**, 127.
Lawn, B.R. and Marshall, D.B. (1979) "Hardness, toughness, and brittleness—indentation analysis," *J. Am. Ceram. Soc.* **62**, 347. Defines the brittleness index (BI).
Munz, D.M., Shannon, J.L., and Bubsey, R.T. (1980) "Fracture-toughness calculation from maximum load in 4 point bend tests of chevron notch specimens," *Int. J. Fracture* **16**, R137. The straight-through crack assumption approach to determination of *Y**. the geometric "constant" in K_{Ic} measurements (cf. Blum *et al.*).
Ridgeway, R.R., Ballard, A.H., and Bailey, B.L. (1933) *Trans Electrochem. Soc.* **63**, 267.
Syed, S.A., Wahl, K.J., and Colton, R.J. (2000) "Quantitative study of nanoscale contact and pre-contact mechanics using force modulation," *Mat. Res. Soc. Symp. Proc.* **594**, 471. Developed the picoindenter—a combination of a nanoindenter and an AFM.
Thoman, D.R., Bain, L.J., and Antle, C.E. (1969) "Inferences on the parameters of the Weibull distribution," *Technometrics* **11**, 445. Used numerical methods to determine *m*.
Weibull, W. (1951) "A Statistical Distribution Function of Wide Applicability," *J. Appl. Mech.* **18**, 293.

WWW

NIST Structural Ceramics Database
(http://www.ceramics.nist.gov/srd/scd/scdquery.htm)
NIST Fracture Property Data Summaries: Oxide Glasses
(http://www.ceramics.nist.gov/srd/summary/glsmain.htm)
NIST Fracture Toughness Data for Ceramics
(http://www.ceramics.nist.gov/srd/summary/ftmain.htm)
NIST Property Data Summaries: Sintered Alumina
(http://www.ceramics.nist.gov/srd/summary/scdaos.htm)
NIST Property Data Summaries: Silicon Carbide
(http://www.ceramics.nist.gov/srd/summary/scdscs.htm)

EXERCISES

16.1 In Figure 16.7 the experimental data for the unstabilized samples deviate from the predicted values for Young's modulus. (a) What do we mean by "unstabilized." (b) How can you account for the difference in the predicted values and experimental values?

16.2 Is Young's modulus affected more by the presence of an intergranular glass phase or an equal amount of porosity? Justify your answer with a suitable calculation.

16.3 Ten rectangular test specimens of MgO were tested in three-point bending. The bars were 1 cm wide and 0.5 cm high and were tested over a 5-cm span. The failure loads for each are given in ascending order: 140, 151, 154, 155, 158, 165, 167, 170, 173, and 180 kg. Calculate the MOR for each sample and the average MOR for this group of samples.

16.4 A commercially available polycrystalline alumina is tested using three different methods: three-point bend, four-point bend, and uniaxial tension. The resulting MOR values are 550, 410, and 175 MPa, respectively. What conclusions can you make about the material from these data?

16.5 The soda-lime silicate glass sample shown in Figure 16.17 was indented with a load of 20 N. Estimate (a) hardness and (b) fracture toughness. (c) How else might you obtain the fracture toughness?

16.6 For the data shown in Figure 16.20 determine the Weibull modulus.

16.7 The following data were obtained in a series of tensile strength tests on polycrystalline silicon carbide specimens (in MPa): 334, 289, 232, 294, 252, 337, 256, 339, 308, 365, 311, 341, 286, 314, 274, 285, 382, 379, 282, 324, 316. (a) Determine the Weibull modulus for these samples. (b) Would you expect the value of m for a set of steel specimens to be higher or lower than the value you calculated in part (a). Assuming that these SiC specimens were made by hot pressing, would you expect m for a series of SiC made by sintering to be higher or lower?

16.8 Calculate using the Voight and Reuss models the bounds for Young's modulus of MgO–Al_2O_3 composites as a function of volume fraction.

16.9 Explain briefly why there is a size dependence for the strength of ceramics but not for metals.

16.10 Sketch stress–strain plots for polycrystalline MgO at (a) 25°C, (b) 1000°C, (c) 1700°C, and (d) 2800°C.